Optics & Laser Technology 186 (2025) 112681

Contents lists available at ScienceDirect

Optics and Laser Technology

journal homepage: www.elsevier.com/locate/optlastec

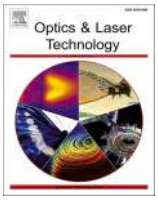

Full length article

Study on laser-assisted joining of titanium (Ti6Al4V) to polyether ether ketone (PEEK) for Enhanced hybrid joints

Silvio Genna [a,*], Patrizia Moretti [a], Gennaro Salvatore Ponticelli [b], Simone Venettacci [b]

[a] Department of Enterprise Engineering, University of Rome Tor Vergata, Via del Politecnico 1, 00133 Rome, Italy
[b] Department of Engineering, University of Rome Niccolò Cusano, Via Don Carlo Gnocchi 3, 00166 Rome, Italy

ARTICLE INFO

Keywords:
Direct joining
Polymers
Diode laser
Titanium
Morphology
Mechanical characterization

ABSTRACT

In the present paper, a 200 W diode laser equipped with a beam expander was adopted to create hybrid joints between pure PEEK polymer and titanium alloy (Ti6Al4V). To this end, a new setup was developed: the laser was equipped with a 5x beam expander, allowing the laser beam a spot of about 30 mm, and the joints were performed in static conditions. The latter allows more efficient control of the joining process, identifying the technological window of processability of the polymer, thus avoiding ineffective heating or excessive degradation during laser-assisted joining operations. Moreover, the adopted setup is very cost-effective from an industrial perspective, depending on the low powers applied, compared with those adopted in the literature. Single-lap joints were carried out in order to study the influence of the laser parameters on the joint strength. Before joining, two different textures were performed on the titanium surface; mechanical tests were carried out to determine the optimal processing conditions, while fracture surface analysis and morphological one were performed in order to better understand the phenomena developing during the joining process. The design of experiments (DoE) approach and analysis of variance (ANOVA) were adopted to identify significant process control factors and analyze how they influence joint performance. From the results, the new setup allows a joint efficiency of about 30 % in the best conditions, a very high value, compared to other traditional joining processes, such as adhesive bonding.

1. Introduction

Polymer-metal hybrid structures have excellent comprehensive properties and have been widely used in aerospace, automotive industry, biomedicine, packaging and other fields [1]. There is a strong demand for dissimilar metal-plastic joints in lightweight design across various engineering fields [2]. This is driven by the need to combine the advantageous properties of both metals and plastics to achieve optimal performance and weight efficiency.

The joining of dissimilar materials, especially in the case of polymers and metallic structures, is significantly challenging due to the difference in the chemical, mechanical, and thermal properties of the materials [3]. Traditionally, metal and polymer or composite are joined together mechanically or using adhesives [4]. Mechanical fastening generally involves external fixings, whether permanent (e.g., joints, rivets, etc.) or not (e.g., screws, nuts, bolts, etc.), which increase the weight [5] and cost of the structure [6]. Furthermore, stress concentrations around joints [5] are particularly high as the load is transferred over only a fraction of the joint area [7].

In addition, mechanical joining processes often require relatively extensive pretreatment, e.g., making holes for inserting the fastening elements. Gluing, on the other hand, allows for an almost uniform distribution of stresses, but the process requires specialized operators and the preparation of the support with long curing times, with a consequent increase in production times and costs. Furthermore, it has a high environmental impact and is affected by environmental conditions, especially humidity and temperature, that contribute to greater uncertainty regarding long-term structural integrity [8]. It should also be noted that these joining techniques have limited use in joining small and/or complex-shaped parts [9]. Therefore, regardless of the process chosen, joints represent one of the greatest challenges in the design of hybrid structures.

Innovative reliable joining processes for such hybrid structures are currently being studied to counteract the limitations described for mechanical or adhesive processes for joining dissimilar materials. The main alternative solutions found so far are: friction-based processes, i.e.,

* Corresponding author at: Via del Politecnico 1, 00133 Rome, Italy.
E-mail address: silvio.genna@uniroma2.it (S. Genna).

https://doi.org/10.1016/j.optlastec.2025.112681
Received 5 December 2023; Received in revised form 16 December 2024; Accepted 20 February 2025
Available online 22 February 2025

friction stir welding [10] and friction assisted ones [11]; laser processes [3], namely laser-assisted direct joining ones [12]; and, more recently, 3D printing processes, in particular fused deposition modeling (FDM) [13] and integrated fused filament fabrication (FFF) and laser-based powder bed fusion (PBF) [14].

However, thermomechanical processes based on friction phenomena produce a poor surface finish in the weld region and lead to high loads. Furthermore, they usually require very rigid locking systems. Regarding 3D printing, the main limitation is due to the choice of both polymer and metal. On the contrary, the use of lasers for joints appears to be a feasible alternative due to their ability to provide instant bonding, very localized heating, absence of vibrations, low residual stresses, flatness of external surfaces, better aesthetics of the joint and low cost, all in one step [15].

As a highly efficient processing technology [2], laser welding has been proven to be a new welding technology with a sound potential in joining hybrid structures compared with traditional adhesives [16], mechanical and other bonding methods [17]. The new automated laser joining technologies for the creation of hybrid metal-polymer components allow the material to be quickly brought to a high temperature, creating joints quickly and without clamping forces, and high automation of the process [15]. Compared to conventional methodologies, such as mechanical joining and gluing, they are easy to automate and do not suffer from problems due to additional weight or the generation of stress concentration phenomena (mechanical joining) [15]. They are not subject to the degradation of adhesives (gluing), and also do not generate environmental sustainability problems [2].

However, the joining presents complex problems, since the materials to be joined present very different behaviors, in both mechanical and thermal terms. Indeed, the effectiveness of the joining depends on the physical, thermal, optical and chemical properties of the materials to be joined: if the polymeric material to be coupled is transparent to the wavelength of the used laser, it will be possible to position it on the side of the laser radiation; this will pass it, heating the underlying material (metal) and the joining will take place by thermal conduction. If the polymer is opaque, i.e., the amount of energy transmitted to the lower layers is very low, a different joining strategy has to be adopted: it is possible to heat the metal by laser radiation and, by conduction, the polymer. Adhesion between parts is then achieved by pressing the components together during laser scanning [18] and a physical or chemical bond between the parts is achieved [19]. Furthermore, some metals show a low chemical affinity with polymers and do not form chemical bonds even when heated to high temperatures. The low chemical affinity can be partly overcome by creating superficial sculpting of the metal surface thanks to the mechanical interlocking mechanism [5,20]: during laser joining the polymeric material, brought to a high temperature, flows inside the grooves, thus creating micro-anchors at the interface with the metal.

To date, numerous literature studies have demonstrated the possibility of joining dissimilar materials through the use of laser technology, such as for example to produce hybrid structures polyethylene terephthalate (PET)-stainless steel (AISI 304) [19], PET-titanium [21], polymethylmethacrylate (PMMA)-AISI304 [22], polytetrafluoroethylene (PTFE)-titanium [23], PET-aluminium [24], and for joining fibre-reinforced thermoplastic [25], such as polycarbonate (PC), polyamide (PA), polyethylene (PE) [26].

In aviation, engineering efforts aim to develop lighter materials without compromising strength and safety [20], and at the same time in a cost-effective manner. One of the main objectives consists of reducing the environmental impact, in terms of CO_2 emissions, and energy saving in the design of aircraft [27], also to reduce as much as possible the cost of fuel consumed and of the construction of the actual aircraft [28]. Among the measures to reduce carbon dioxide emissions, one possible solution is reducing the weight of the aircraft's primary structure [29]. In fact, lighter materials reduce the load, resulting in lower fuel consumption and therefore lower CO_2 emissions [30]. So far, research has focused attention on composite materials to replace traditional metal alloys [27], i.e., aluminum [30], magnesium, steel and titanium alloys [31], for the intelligent design of aircraft [29], with the aim of improving fatigue resistance [32].

In LEO (Low Earth Orbit) and aerospace applications, an essential property is the watertight and outgassing [33]. In this regard, about metal-polymer joints, the watertightness is related to the absence of interconnected voids between the substrate and the polymer, which could be problematic in the event of strong thermal cycles as an increase in temperature can cause pressures that could contribute to the detachment of the materials. PEEK, thanks to its excellent mechanical properties and lightness [30], is the most widely used polymeric material in structural applications. Studies show that it is possible to create joints with good adhesion properties to the metal substrate [34], after treating the surfaces of the latter to make it hydrophilic, during the fusion phase in the laser joining process, thus preventing the presence of gaps [35]. The main parameter for choosing the metallic side of the joint in the structural sector is the relationship between weight and mechanical properties: low weight combined with high mechanical stiffness and ultimate yield strength [36]. Resistance to the space environment and the ability to manage thermal loads is generally entrusted to protective and/or thermal insulating layers [37]. Titanium alloys, like magnesium alloys, have excellent structural and lightweight properties; however, their use is limited by the difficulty of manufacturing and processing the products [36]. They are more extensively used in the aeronautical sector, where the structural stresses are greater than those found in small satellites in LEO [34]. Titanium alloys have in fact many advantages, such as a good fracture point, good resistance to fatigue and corrosion, boast superior resistance to high temperatures, and today represent one of the most important classes of structural materials for the body, frame, and of gas turbine engine of aircraft, both for civil and military use. The main disadvantage concerns the processing costs. From this perspective, their combination with thermoplastic polymers or thermoplastic matrix composites can form a new light and resistant system [38], which can be used in low and high velocity impact applications, thus introducing new hybrid laminates with properties optimized for aeronautical applications. In this context, technopolymers represent advanced plastics with superior properties as compared to traditional plastics. They are designed to withstand extreme heat and mechanical stress. Among these, PEEK is used in the aerospace industry, together with other polymeric materials represented by PFPE (perflioroalkulpoluether); PTFE (polytetrafluoroethylene); Kapton (polyoxydiphenylene-pyromellithimide); PP (polypropylene); PE (polyethylene).

In this framework, the present study investigates the laser-assisted joining of titanium alloy (Ti6Al4V) and PEEK, topic still little addressed in the literature and thus worthy of more in-depth investigation. In fact, no literature work has studied hybrid joining between pure PEEK polymer and titanium alloy (Ti6Al4V) so far. Previous literature works [39–43] have focused instead on similar hybrid joining between continuous carbon fiber-reinforced polyether ether ketone (CCF30/PEEK) and titanium alloy (Ti6Al4V), realizing high-performance joints [39], building effective micro-mechanical interlocks between metal and fiber-reinforced plastic [41]. Such works have identified mechanical locking, either due to the roughness of the specimens or the surface texture generated, as a key mechanism for joining specimens [42]. Only Tan et al. [40], as well as Zou et al. [43], have also considered the role of chemical bonding, in terms of chemical reactions between the fiber-reinforced plastic and the metal material, in the context of adhesion mechanisms at the interface, studying the formation of new chemical phases/structures by Energy Dispersive Spectrometer (EDS). In the present research, joint tests were carried out in order to study the joining mechanisms underlying the hybrid metal-polymer laser-assisted joining and the influence of the laser parameters on the joint strength. To this end, a diode laser equipped with a fixed-point beam expander (further novelty of the paper) that allows the beam a spot of about 30 mm in static conditions was adopted. In contrast

to the work done in the previous literature papers cited [39–43], the adoption of such a laser system can be very cost-effective from an industrial perspective, depending on the low powers applied, compared with those of the latest generation lasers. A dedicated clamping system has been designed and fabricated by additive technique (Fused Deposition Modeling) to assist joining by applying external consolidation pressure between the two specimens to be joined. The design of experiments (DoE) approach and analysis of variance (ANOVA) were adopted to identify significant process control factors and analyze how they influence the joint performances. The following parameters were studied: the ultimate shear force (UFS), the metal-polymer joined area (A), and the shear strength (τ). In addition, the cross sections were observed by means of a metallographic microscope, while the morphology of the fractures was observed by means of a 3D digital microscope. Finally, Energy Dispersive X-ray Spectroscopy (EDXS) was used to determine the elemental composition of the materials present on the PEEK and titanium surfaces after shear tests, thus the role of chemical bonding in the overall anchorage between the two materials, according to [40,43]. Before performing joints, laser texturing was performed on the titanium surface, as operated in only [39,41] of the previous cited papers, however focused on CCF30/PEEK-Ti6Al4V. Joints were then made by applying two different powers of the laser beam using a diode laser (i.e., 150 W and 200 W). From the results, the optimal processing conditions were detected, from fracture and morphological analysis, the phenomena developed during the joining process were studied, and, from EDXS analysis, the contribution of chemical bonding was evaluated as part of the adhesion mechanisms at the interface. The aim was to identify the technological window of processability of the polymer, in order to avoid its ineffective heating or excessive degradation in laser-assisted joining operations, and thus ensure a mechanically strong and chemically stable joint as well.

2. Experimental procedures

2.1. Materials

The investigated materials are PEEK 1000 by Ketron (5 mm thick) to be joined with 2 mm thickness titanium alloy Grade 5 (Ti6Al4V). PEEK is one of the most used materials in LEO missions, in the range between 400 and 2,000 km altitude. PEEK 1000 by Ketron stock shapes are produced from virgin polyether ether ketone resin, offering the highest toughness and impact strength of all Ketron PEEK grades. PEEK is a semi-crystalline polymer, which shows high stiffness and hardness and a unique high tensile resistance and fatigue strength. It is resistant to high-energy radiation, abrasion and wear; it is a good electrical insulator even at high voltages and it shows very good mechanical properties and exceptional dimensional stability even in continuous operation at high temperatures (up to 250 °C). It is processable in conventional techniques such as injection molding, compression molding and extrusion. Can be mixed with PTFE for applications requiring good wear and friction properties. It is used in nuclear environments, oil and geothermal wells, chemical industries and high-pressure valves. Unlike many other engineering plastics, PEEK is completely recyclable, mechanically or as a raw material. PEEK 1000 by Ketron was characterized according to a previous study [44], applying the same test methodology used for thermoplastic samples in high density polyethylene (HDPE) and polyethylene terephthalate (PET), but with different parameters. Specifically, the samples adopted in this research project were obtained from the available slabs using the Stepcraft D840 CNC machine equipped with a Ø2 mm 828 cutter supplied by MJ CNC Automation. The cutting parameters were appropriately chosen to ensure the best side surface quality along with maximum production speed: the cutting speed was set at 20000 rpm, the depth of cut at 1 mm (1 pass), and the feed rate at 350 mm/min.

The mechanical characterization of the polymer specimens was completed through tensile tests (according to ASTM D638), performing 5 repetitions of the test, employing a crosshead speed of 5 mm/min, and acquiring the Young's Modulus (*E*, GPa), the Ultimate Tensile Strength (*UTS*, MPa), the strength at break (σ_R, MPa), the yield strength (σ_Y, MPa) and the elongation at break (ε_R, %), as reported in Table 1. Instead, the thermal characterization involved: (i) the identification of the main thermal properties through differential scanning calorimetry (DSC) and (ii) the evaluation of the degradation of the polymers with the temperature through the thermo-gravimetric analysis (TGA), whose results are instead reported in Table 2. Specifically, the average values of the melting temperatures (T_m), of the crystallization temperatures (T_c), and of the degrees of crystallinity (X_c), were calculated from DSC thermal cycling (in the range 80–400 °C) as averages of the values acquired before and after laser irradiation of PEEK (at 40 W for 60 s). The glass transition temperature (T_g) was acquired on the irradiated PEEK. The "onset" temperature is extrapolated according to ISO 11358–1 ($T_{on.E}$), as in [44].

Table 1
Mechanical properties of PEEK.

Mechanical properties	Symbol	Value	Unit
Elastic Modulus	E	3.44 ± 0.08	GPa
Ultimate Tensile Stress	UTS	103.21 ± 1.14	MPa
Strength at break	σ_R	57.65 ± 6.06	MPa
Yield strength	σ_Y	41.52 ± 2.81	MPa
Elongation at break	ε_R	11.74 ± 0.33	%

Table 2
Thermal properties of PEEK.

Thermal properties	Symbol	Average Values	Unit
Melting temperature	T_m	341.15 ± 2.42	°C
Crystallization temperature	T_c	293.41 ± 3.60	°C
Crystalline fraction	X_c	33.69 ± 6.48	%
Glass transition temperature	T_g	163.95	°C
Onset temperature	T_{on}	563	°C
Residue	–-	47.7	%

Titanium alloys have excellent structural and lightweight properties; however, their use is limited by the difficulty of manufacturing and processing the products. They are more extensively used in the aeronautical sector, where the structural stresses are greater than those found in LEO CubeSats [34]. The chemical composition and the mechanical properties of titanium sheets are listed in Table 3.

2.2. Laser system

During laser-assisted joining tests, a 200 W diode laser (DLR-200-AC, by IPG) was used with a fundamental wavelength of 975 nm. The joining setup, illustrated in Fig. 1, includes a diode laser, a collimator (100 mm focal length) mounted at the end of the fiber optic cable, a beam expander (5 ×), a clamping system and the FLIR A665sc thermal imaging camera for temperature monitoring. The laser beam was characterized by a circular shape of about 6 mm in diameter with low beam quality (BPP = 22 mm × mrad), therefore a circular shape of about 30 mm was obtained after the beam expander. The titanium sheet was placed at the laser beam side; thus, the underlying PEEK was heated by heat conduction through the aluminum thickness. The clamping system was ad-hoc designed and 3D printed by FDM technique; it is able to apply a clamping pressure of about 1.0 MPa, maintained for the entire joining time, then for at least another 30 s to give the joint itself time to cool and consolidate. The 3D printed part was designed to reduce heat loss by conduction and to homogenize the temperature of the joint.

2.3. Experimental procedures

The PEEK, opaque to the wavelength of the laser used, was placed on

Table 3
Chemical composition and mechanical properties of titanium alloy (Ti6Al4V).

Element	Fe	C	N	H	O	Al	V	Titanium	Other
Min (%)	0.110	0.015	0.009	0.0085	0.138	6.28	3.99	Remainder	<0.1
Max (%)	0.112	0.013	0.007	0.0087	0.135	6.28	3.85		<0.4

Mechanical properties	Tensile strength (MPa)	Yield Strength, 0.2 % (MPa)	Elongation (%)
Longitudinal analysis	1048	972	13.50
Transverse analysis	1035	1019	12.50

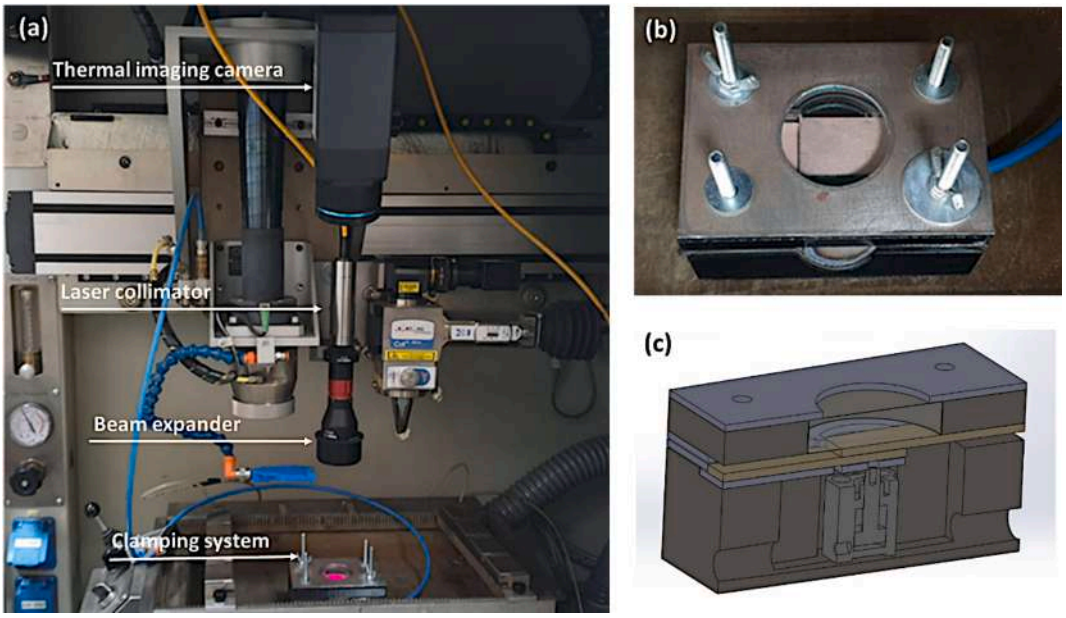

Fig. 1. Joining setup: (a) overall view; (b) detail of clamping system; (c) cross-section of the clamping system.

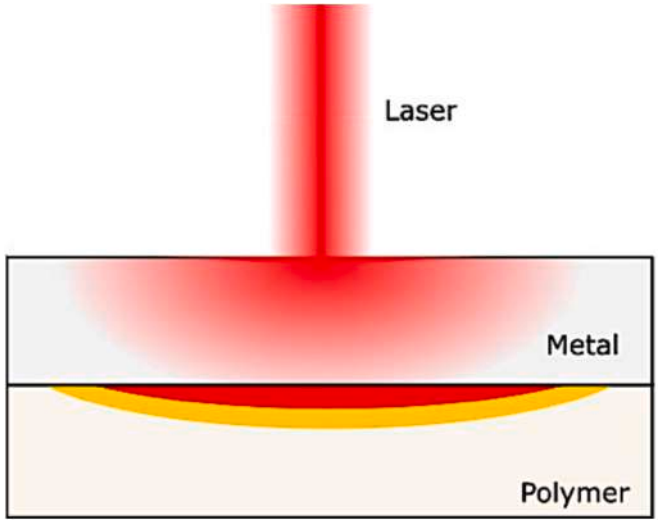

Fig. 2. Heating mechanism.

the opposite side of the laser beam (i.e., on the bottom side): the metal was directly irradiated by the laser, it heated and, by conduction, melted the polymer. The heating mechanism is schematically reported in Fig. 2.

An infrared camera was performed to acquire the temperature of the central point of the irradiated (upper) titanium surface during the joining operations. During the operations, an acquisition rate of 30 Hz and a temperature range of 50 – 650 °C was adopted. The camera was placed at an angle of 80 degrees with respect to the titanium sheet at a distance of almost 400 mm. The adopted emission coefficient was set equal to 0.85 in the IR camera, as suggested by the manufacturer, for a correct temperature measurement. Laser-assisted joints were conducted by means of a stationary laser beam to produce spot joints.

Preliminary joining tests, performed on the "as-received" titanium sheets indicated a poor adhesion between the substrates due to the poor surface chemical affinity of the materials. Thus, laser surface texturing (LST) was performed on the titanium substrate to increase the mechanical strength of the joints. To this end, the titanium specimens' surface was treated by laser ablation to produce grooves [45]. The texturing was produced by means of a fibre laser (Yb:YAG) (model YLP-RA30-1–50-20–20 by IPG Photonics) equipped with a galvanometric scanning head (supplied by LASIT SpA), with a focal spot of about 80 μm, average power of 30 W, wavelength of 1064 nm, focal length of 160 mm, pulse frequency of 30 kHz, pulse duration of 50 ns, scanning speed of 2000 mm/s, mode TEM 00, M^2 1.2 ÷ 1.5 [46]. Aimed to obtain grooves able to embed the melted polymer, and to detect the best groove geometry, two different textures were designed: the first consisted of two adjacent lines, spaced 20 μm apart, with a hatch distance of 0.5 mm; the second of three adjacent lines, spaced 20 μm apart, with a hatch distance of 1.0 mm. To ensure a depth of about 40–50 μm, same for all texturing lines, each texture was repeated 30 times, i.e., the scanning path of the laser beam was performed 30 times in succession, always moving in the same verse, along the same direction. Top and 3D views of the laser textures produced on the titanium sheet are reported in Fig. 3 (textures A and B). Before joining, the surfaces were cleaned by means of an ultrasonic bath of water (for an immersion time of 10 min) to remove

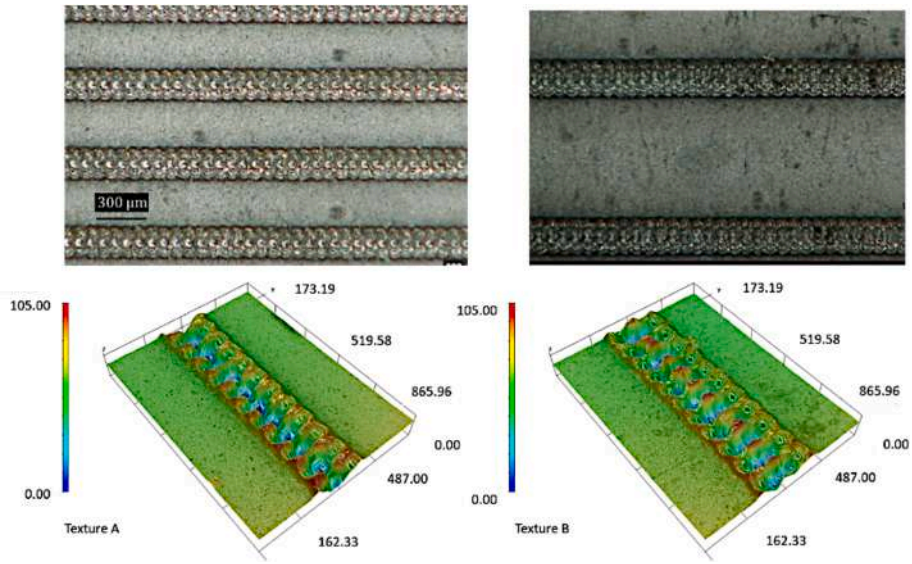

Fig. 3. Top and 3D views of textures A and B on titanium.

Table 4
Texture A and B processing parameters (titanium).

Main texture characteristics	Symbol	Texture A	Texture B	Unit
Hatch distance	Hd	0.50	1.00	mm
Distance between peaks	d1	176.01	220.96	µm
Distance/width between the burrs	d2	227.56	292.99	µm
Burr height	h1	16.13	16.81	µm
Depth	h2	46.67	50.38	µm
Arithmetic mean surface roughness	Ra	7.64	10.83	µm
Mean surface roughness depth	Rz	23.67	30.03	µm

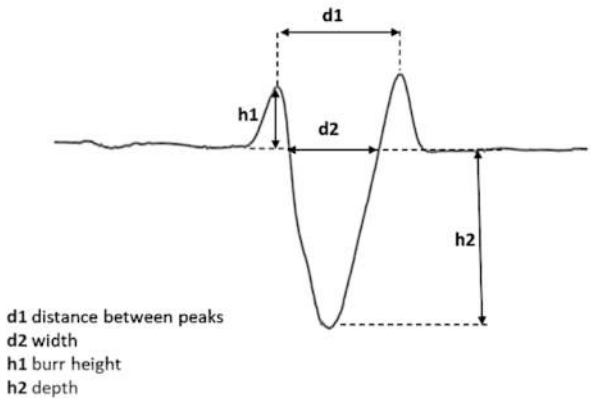

Fig. 4. Characteristics of the engraving profile.

Table 5
Factorial plan: control factors and their levels.

Control factors	Level 1	Level 2
P [W]	150	200
t [s]	20	30
Texture	A	B

the eventual debris.

A digital microscope (HIROX, KH-8700) equipped with a 2.11 megapixel CCD sensor was used to perform measurements of the grooves' geometry (Fig. 3). Table 4 and Fig. 4 report the main characteristics.

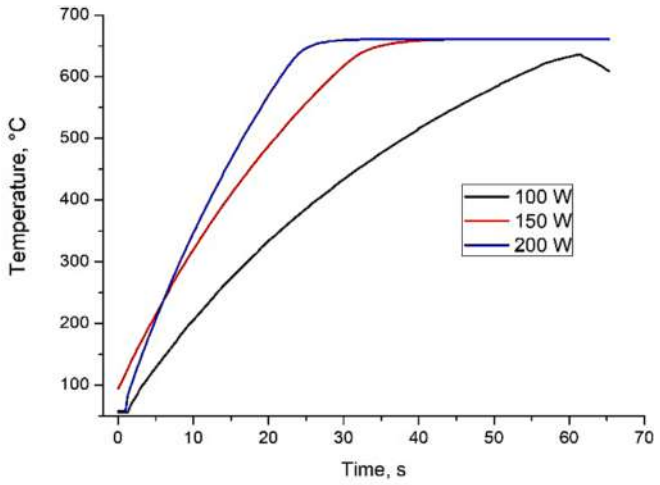

Fig. 5. Temperature measured on the irradiated titanium surfaces at 100 W, 150 W, and 200 W.

A full factorial plan with 3 factors (i.e., laser power, irradiation time, and metal surface texture) at 2 levels for each factor, for a total of 8 different combinations was developed and tested; the tests were replicated 3 times for a total of 24 specimens. The process parameters, i.e., the control factors, are summarized in Table 5. The experimental plan was fully randomized.

The control factors levels were chosen in such a way as to maintain the temperature above the melting temperature and below the onset temperature of the polymer: the operating time and laser power range were established considering the polymer melting and onset temperatures (Table 2) and the temperature reached by the titanium during the joining operation. To this end, individual titanium plates, i.e., without coupled polymer sheets, were preliminary irradiated by the laser at different powers and their superficial temperature was acquired; the temperature reached during these preliminary tests (in correspondence with the central irradiated area) is shown in Fig. 5.

It should be considered that the temperature recorded does not refer to the metal-polymer interface but to the upper surface of the metal part. In [47] the superficial temperature was approximated to the temperature reached at the metal-polymer interface during the joining

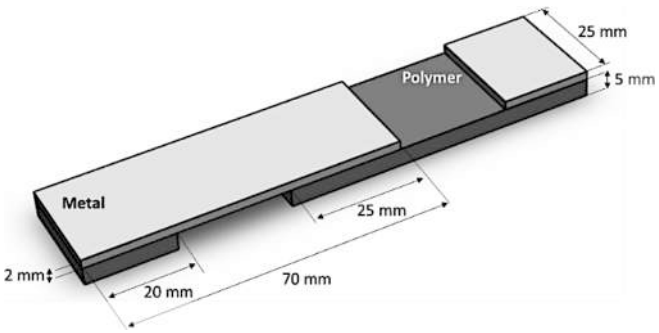

Fig. 6. Schematic of the hybrid joint.

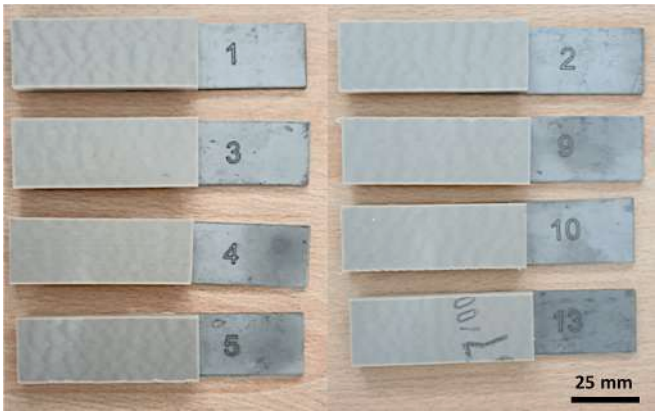

Fig. 7. PEEK – titanium joints.

operations since the metal part of the joint was aluminum. In the present study, the metal part is a titanium alloy that shows a thermal conductivity of 2 orders lower than the aluminum one.

From Fig. 5, it appears that the ideal time interval to reach the processing temperature for titanium-PEEK was between 10 and 20 s. Within this range, excluding the lower radiation power (i.e., 100 W), the maximum temperatures reached on the surface are in the range of 320 – 580 °C. From preliminary tests based on the thermal measurements, it was decided to adopt in the factorial plan the following values: 20 s and 30 s. Given the importance of reducing process times in the industry, it was decided not to perform low power (i.e., 100 W), since the joining time was over 60 s.

2.4. Realization and mechanical characterization of hybrid joints

The joints' mechanical behavior was assessed by single-lap shear tests. The schematic of the specimen is reported in Fig. 6: the plates are both 70x25 mm^2 in dimensions and 5 mm and 2 mm in thickness, respectively for the polymer and the metal. Textures A and B were created on a 25x25 mm^2 metal surface to promote the hybrid metal-polymer joining. Fig. 7 depicts the joints obtained by implementing the factorial plan, before applying the alignment pads.

Tests were performed under a constant crosshead speed of 1.27 mm/min, at room temperature, by means of an MTS Insight 100 Material Testing Workstation, equipped with a load cell with 50 kN full scale. The test specifications refer to the ASTM D3163 standard, relating to the determination of the resistance of rigid plastic joints glued and subjected to tensile loading by means of shear tests. The standard was modified by replacing the adhesive with a different adhesion process (i.e., laser-assisted joining). According to the standard, the joints were considered rigid, and non-deformable, thus, no bending moment was generated.

After the test, images of the detached surfaces and the fracture

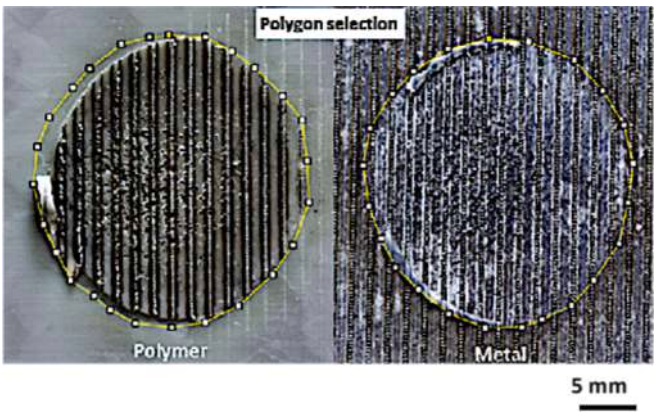

Fig. 8. Schematic of the joined area measurement process after the single lap shear test on the top surface of PEEK (titanium-PEEK, 150 W, 20 s, texture B).

morphology were acquired using a high-resolution digital camera (Canon D60, 100F28 macro lens) and processed using Image-J software for calculating the residual areas (A): the polygonal selection was performed according to the schematic of Fig. 8. It is worth noting a smaller apparent residual joined area on the polymer side than that be visible on the metal. The comparison of the residual areas present on both components of the joint is therefore fundamental to determine the real extension of the joined area.

To assess the main joining mechanism, cross-sections along additional joints (one for each condition of the factorial plan) were performed in the middle by means of an abrasive cutting blade and prepared according to standard procedures for metallographic specimen preparation. The cross sections were observed by means of a digital microscope (KH-8700 by Hirox).

According to the standard, the apparent shear strength of the joints (τ) was evaluated by dividing the maximum load (UFS) measured during the test by the joined area A:

$$\tau = \frac{UFS}{A} \tag{1}$$

Three repetitions were performed for each condition and the average and standard deviations were calculated. Following the shear tests, EDXS analysis (Gwonseon-gu, Suwon, South Korea) was used to determine under a scanning electron microscope the elemental composition of materials present on the PEEK and titanium joint surfaces.

3. Results and discussions

3.1. Mechanical behavior of the joints

Fig. 9 depicts the typical force–displacement curves obtained by the single-lap shear test for the Ti-PEEK joint. In Fig. 9a, the test was performed at high laser power (i.e., P = 200 W) and in Fig. 9b at medium power (i.e., P = 150 W); for both images, it can be noted the difference in the peak load between the solid and dashed curves, which indicates the notable influence of the irradiation time on the joining process. This can be addicted to the reached temperature; the higher the time, the higher the temperature and, consequently, the PEEK better melts and fills grooves, because less viscous at higher temperatures. Similar considerations can be drawn in the case of laser power: the higher the power, the higher the force. In fact, the hindmost of the curve reaches about 6 kN in the case of 200 W at 30 s. On the other hand, the texture seems to be less relevant, since the lines red and black ones reach almost the same values. However, a light influence is visible: texture A seems to ensure a small increase in force. This can be addicted to the almost double number of grooves present in texture A as referred to the texture B; nevertheless, the latter is characterized by larger grooves, which can

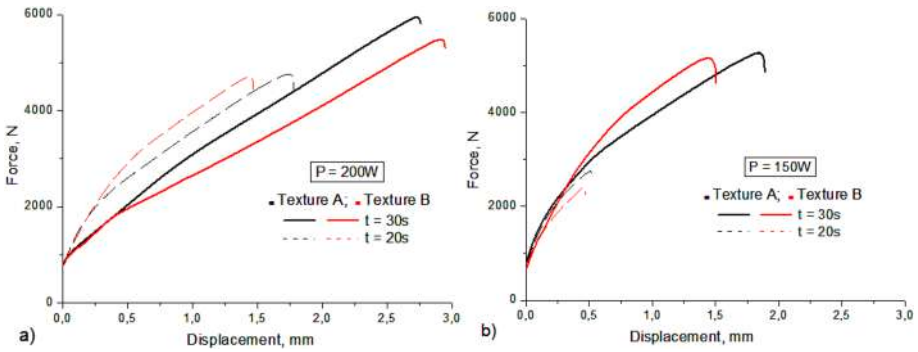

Fig. 9. Force-displacement curves of titanium-PEEK joints irradiated at: (a) P = 200 W; (b) P = 150 W.

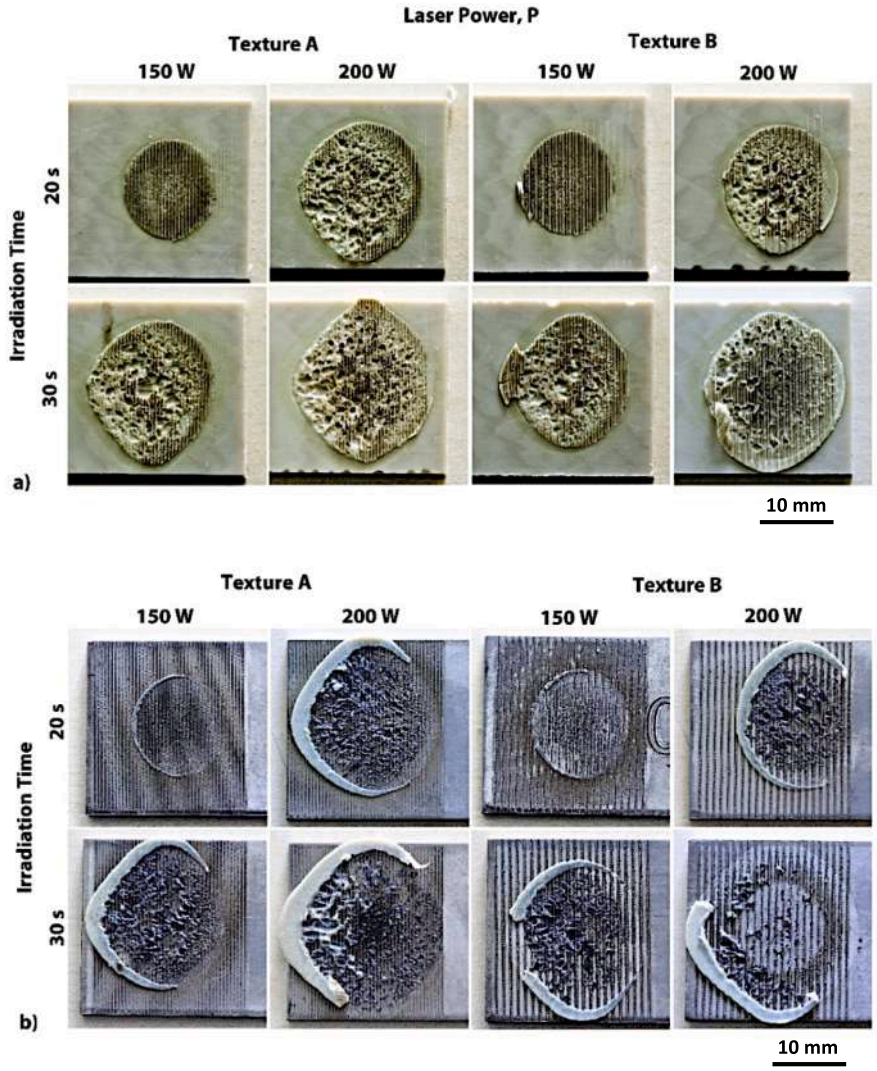

Fig. 10. Joined area after single-lap shear test on side of (a) PEEK side and (b) titanium side, for different laser power (150 W, 200 W), time (20 s, 30 s) and texture (A, B).

promote the polymer's filling. Consequently, the last-mentioned effect can compensate for the fewer grooves.

Overall, all the joining conditions led to the successful joining of the substrates; this means that the factorial plan was well-designed. In addition, the force trends exhibit a ductile behavior of the joints produced with higher power (i.e., 200 W) and longer irradiation time (i.e., 30 s). The joint produced with P = 150 W and t = 20 s (Fig. 9b) showed more brittle behavior than the others.

Regarding the influence of the process parameters (i.e., P, t, and texture) on the apparent shear stress (τ), the latter requires the calculation of the metal-polymer joined area (A). Fig. 10 shows the surfaces of polymer and titanium after the shear tests. From the images, the influence of the process parameters on the joined area A is visible. As can be inferred, higher laser energy (i.e., major laser power and joining time)

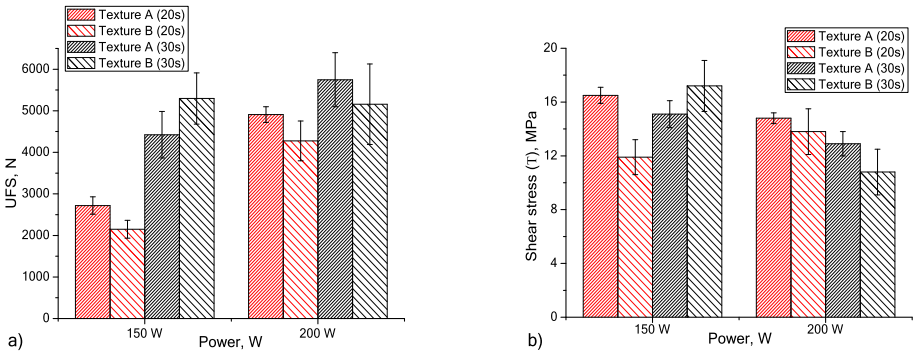

Fig. 11. Ultimate shear force UFS (a) and apparent shear stress τ (b) at the different powers (i.e., 150 W and 200 W) as a function of the texture and irradiation time.

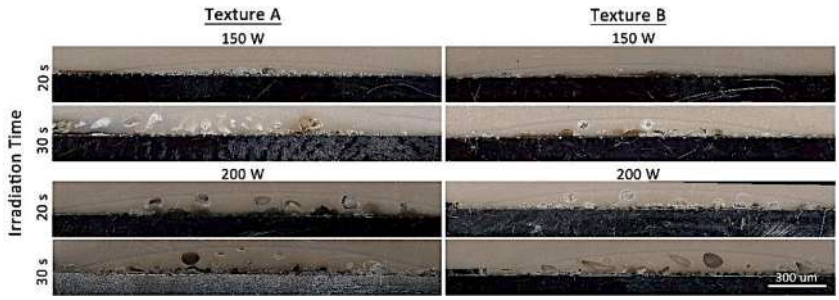

Fig. 12. Cross-sections of the joints at different process conditions.

leads to an enlargement in the joining area. Furthermore, in all the conditions, except the lower energy one (i.e., P = 150 W, t = 20 s), a lot of bubbles are present; this can be mainly addicted to the presence of moisture in the polymer [12], but not completely, as it is also due to the presence of plasticizers within the PEEK. During the joining/heating, the bubbles are nucleated, grew, and coalesced. These reduce the effective

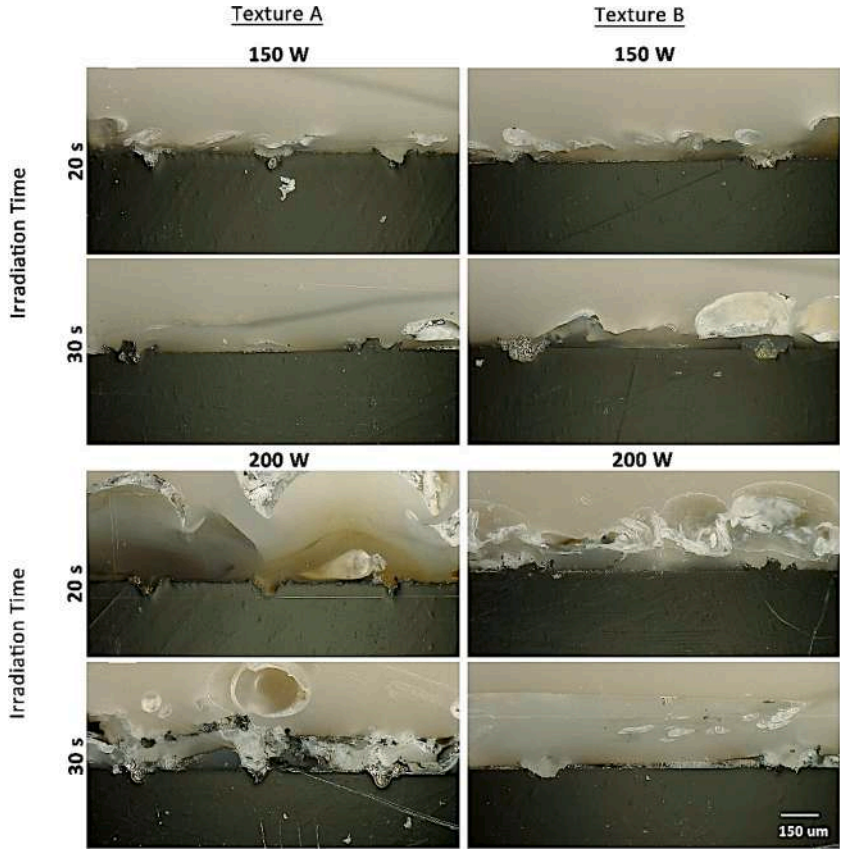

Fig. 13. Cross-sections magnification: main joining mechanism.

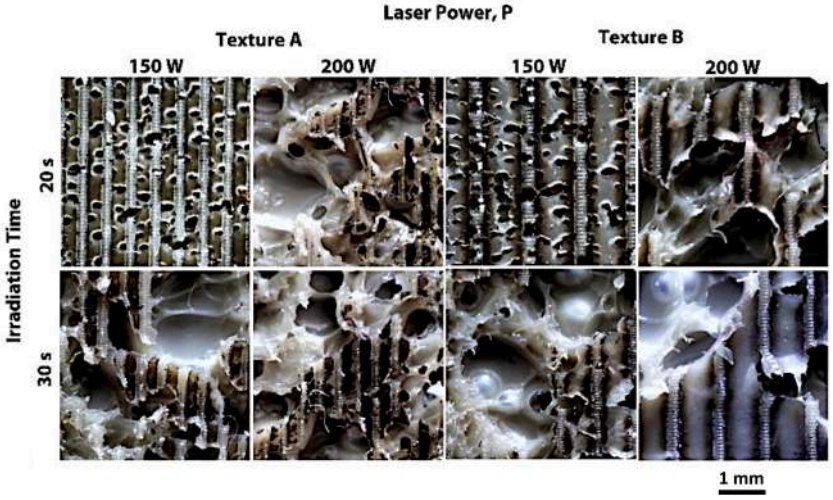

Fig. 14. Morphology of PEEK surfaces after testing.

joining area and promote the stress concentration during loading conditions. For further details, please refer to the analysis of the morphology and fracture surfaces.

Fig. 11 illustrates UFS and τ for all the tested conditions; the error bars show the standard deviation. The UFS value increases at the highest power (i.e., 200 W) and increases as the irradiation time increases from 20 s to 30 s (Fig. 11a). The apparent shear stress (τ) shows an opposite behavior: it generally decreases at the radiation power increasing, indicating a deterioration phenomenon at the level of the interface metal-polymer when higher temperatures are reached (Fig. 11b). To understand this phenomenon, please refer to the analysis of the fracture surface. The only exception to these considerations can be referred to texture B, for the case where the energy input is lower, i.e., for 20 s and 150 W control factors: the apparent shear stress (τ) is higher at 200 W power, underlining a better anchorage of the polymer at the interface with the metal, compared to what happens at 150 W power, a configuration for which the lowest value among all of UFS is instead recorded (since the energy supplied to the metal is not enough to make the polymer flow well inside the grooves created and fill them, being significantly larger than for texture A). In addition, the texture seems to affect less the UFS and τ parameters: the change from texture A to B generally results in a slight decrease in UFS and τ, in agreement to the statements about Fig. 9. The apparent shear stress reached the maximum value of about 18 MPa (for P = 150 W and t = 30 s), which corresponds to UFS ~ 5.5 kN.

The joint efficiency can be calculated as the ratio of the strength of the joints (i.e., shear strength) to the strength of the base material. According to Von Mises criteria, the shear strength of the base material τ max can be calculated as:

$$\tau_{Max} = \sigma_{Max}/\sqrt{3} = 103MPa/1.732 = 59.5\text{MPa} \quad (2)$$

Thus, under the best conditions, the joint efficiency, calculated as the ratio of the shear strength of joint (~18 MPa) to that of base polymer (~59.5 MPa), reached about 30 %.

3.2. Analysis of joint morphology

To further understand the influence of the process conditions on the shear strength of the joints, the morphology of the joints was analyzed. Fig. 12 represents the cross-sections of the specimens at the different process parameters. At the metal-polymer interface, textures A and B cavities are visible along the entire sampling length. It is possible to observe a change in color in the area that reached the highest temperatures (for P = 200 W). In particular, for more drastic irradiation conditions, within this region underlying the metal/polymer interface, the formation and growth of the bubbles can be observed. These bubbles, present at the metal-polymer interface and within the polymer substrate, resulted in a mixed fracture mechanism. Thus, the increase in the heating time can have a detrimental effect on the strength of the joints [11]. The presence of bubbles influences the strength of the joints, as they reduce the resistance area and induce stress concentration [48]. The presence of bubbles determines a sort of fracture line in the PEEK bulk; as a result, there are a lot of residues of PEEK on the titanium substrate (Fig. 10b). These factors decreased the average value of the shear stress from the maximum value of about 18 MPa to a minimum value of about 12 MPa obtained under the most drastic irradiation conditions (i.e., 200 W and 30 s). Anyway, it is worth noting that these shear stress values are comparable to those that can be obtained with aeronautical structural bonding [49].

Fig. 13 shows the main joining mechanism: during the laser heating, the polymer melts and fills the textures' grooves on the metal surface. This makes the mechanical interlocking mechanism effective, which can increase the joint strength. However, due to polymer degradation, excessive heating conditions can lead to defects at the interface. The latter is due to the presence of moisture in the polymer: some areas are rich in bubbles. The growth of bubbles explains the decreasing trend of the parameter τ generally observed following the shear test at the highest power (i.e., 200 W). This mechanism is also clear by observing the magnification of the fractured surface of the polymer side, reported in Fig. 14: in all the images the grooves imprints are clearly visible, a sign of good adhesion. At high energy (i.e., high power and time) the voids due to the bobbles are clearly visible, indicating a decrease in the effective joint area.

The efficiency achieved by the joint is equal to ~ 30 %. Such a value is very high, compared to other joining processes, such as adhesive bonding. Generally, a minimum shear strength of 7 MPa is required for structural adhesives [49]. Therefore, in some contexts, laser-assisted joining can be considered a valid alternative for creating hybrid materials.

3.3. SEM-EDX of the fracture surface

Two Ti6Al4V-PEEK joints obtained at the mildest and most drastic irradiation conditions were selected to discuss the EDXS analysis: 150 W, 20 s (texture A) and 300 W, 60 s (texture B). Shear tests of the joint obtained at 150 W and 20 s show an excellent shear force (τ) of about 17 MPa and a low UFS value of about 2750 N. Shear tests for the joint at 200 W and 30 s give lower value for τ, i.e., of about 11 MPa, while very high for UFS, i.e., of about 5 kN. The trend of the two parameters can be

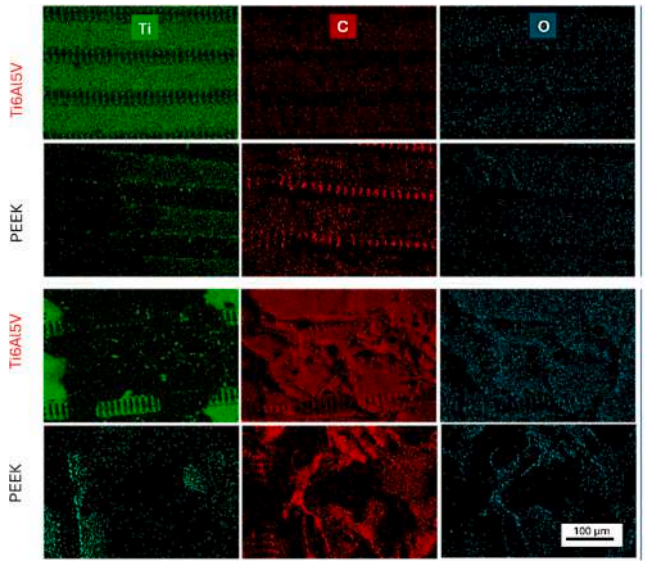

Fig. 15. EDXS scan results of mapping elements on Ti6Al4V and PEEK fracture surfaces.

explained by the relation (1), where parameter A is visibly lower under the milder irradiation condition (please refer to Fig. 10). In this case, since the area is small, the same force results in a higher stress concentration, i.e., it is concentrated in a small region of material, which leads to an increase in shear stress τ, but the joint can only withstand a relatively low total force (UFS) before failure.

Under the most drastic irradiation condition, a larger joint area is observed. In this case, the applied force is distributed over a larger area, reducing the apparent stress per unit area. The shear stress τ is diminished, but the UFS increases as the larger contact area supports more total force.

Fig. 15 shows the element distribution of the fracture surface of Ti6Al4V and PEEK under the two selected irradiation conditions (i.e., 150 W and 20 s, 300 W and 60 s, respectively). EDXS analysis of the fracture surface can provide a better understanding of the chemical and physical mechanisms involved in the joining process.

The results in Table 6 suggest a material transfer between the two surfaces, which can promote good adhesion. The massive presence of carbon on the texture B of the titanium (~71 % Ti) is also visible when observing the joining areas after the shear test (please refer to Fig. 10b). We observe the presence of Ti adhered to the PEEK surface, particularly under the milder radiation condition (5.9 % Ti and 0.4 Al), which we associated with a very high shear strength. This finding may be related to a stronger mechanical and/or chemical adhesion between the joint surfaces, whose connection resisted well to failure.

It is possible to observe oxygen on the surfaces of PEEK and attribute this mainly to the oxidation of the carbon contained in the polymer itself. Under the most drastic irradiation condition, a certain percentage of oxygen is observed (18.1 %), slightly lower than under the mildest irradiation condition (23.9 %).

This phenomenon can be explained by considering the vaporization mechanism of the moisture content within the PEEK under most drastic irradiation conditions. Furthermore, at elevated temperatures, PEEK is subject to degradation, which results in the release of oxygen as a gas and, thus, a reduction in the amount detected. Degradation was indeed observed with the formation of bubbles within PEEK. Under milder conditions, oxidation prevails, leading to a higher amount of oxygen detected.

Under milder irradiation condition, the presence of 23.1 % of oxygen on titanium suggests that the laser effect is also capable of causing metal oxidation. The improved adhesion between PEEK and Ti6Al4V is probably due to the combination of surface oxidation of Ti and PEEK. It results in the formation of reactive chemical groups that can bond together. Titanium is very reactive with oxygen and when exposed to air or heat-treated forms a titanium oxide (i.e., TiO_2) layer on its surface. This titanium oxide layer can facilitate adhesion with polymers, such as PEEK, through various mechanisms: (i) hydrogen bonds: titanium oxide can form hydrogen bonds with the ketone groups (−C=O), present in the chemical structure of PEEK; (ii) chemical interaction: the oxide layer can promote the formation of covalent bonds or strong van der Waals interactions between the oxidized metal surface and the polymer, improving adhesion; (iii) oxygenated functional groups, such as hydroxyl (–OH), carbonyl (−C=O), or carboxyl (–COOH) groups, can be formed on the surface of irradiated PEEK. These groups can chemically interact with the oxidized surface of the titanium.

Similar laser joint studies between Ti6Al4V and carbon fiber-reinforced PEEK analyzed their interface surfaces and demonstrated the mutual diffusion of the elements at the joint. They could be inferred that Ti, Al and O could be precipitated in reaction at the joint interface, and bonds could be formed by chemical reaction. According to previous literature works of Tan et al. [40], as well of Zou et al. [43], the reaction energy of Al and Ti elements with C and O was relatively low, and it was promising to form the stable chemical bonds of Ti-O, Ti-C, and even Al-O-C in heat processing.

Aluminum in the Ti6Al4V alloy is very reactive and easily forms aluminum oxide (Al_2O_3) on the surface, which can interact with PEEK similarly to titanium oxide. Vanadium oxide (V_2O_5), if present, may also contribute to adhesion through electrostatic or chemical interactions with the PEEK oxide groups. Under milder irradiation condition, the surfaces were not excessively damaged, resulting in a good compromise between surface modification (e.g., the creation of an oxidized layer) and joint integrity. This may have facilitated the transfer of titanium onto PEEK (5.9 %) and, at the same time, improved the adhesion between the two materials.

In conclusion, while the laser texturization treatment on the metal can favor mechanical anchorage, laser irradiation can influence the adhesion between PEEK and Ti6Al4V by favoring chemical reactions. The presence of Ti on the polymer after the shear test is a good indicator to assess the adhesion and thus the quality of the joint obtained. By investigating the fracture surface, it was possible to study the adhesion and quality of the joint, obtaining results consistent with analysis conducted in similar studies at the polymer-metal interface.

Table 6
Element content on Ti6Al4V and PEEK fracture surfaces illustrated in Fig. 15.

Weight % of the elements under mild laser irradiation condition: 150 W, 20 s									
Ti6Al4V (texture A)					**PEEK**				
Ti	O	Al	V	C	Ti	O	Al	V	C
67.7 ± 1.2	23.1 ± 1.3	4.0 ± 0.1	3.1 ± 0.2	2.0 ± 0.3	5.9 ± 0.2	23.9 ± 1.0	0.4 ± 0.1	–	67.0 ± 1.0
Weight % of the elements under drastic laser irradiation condition: 200 W, 30 s									
Ti6Al4V (texture B)					**PEEK**				
Ti	O	Al	V	C	Ti	O	Al	V	C
12.1 ± 0.1	13.9 ± 0.4	0.7 ± 0.0	0.6 ± 0.0	71.3 ± 0.3	2.0 ± 0.1	18.1 ± 0.8	–	–	77.5 ± 0.8

Table 7
Results of the ANOVA analysis on the UFS, A, and apparent shear strengths (τ) in terms of the p-value. The significant control factors (p-value < 0.05) are shown in bold.

	UFS [N]	A [mm^2]	τ [MPa]
Source	*p-value*	*p-value*	*p-value*
P [w]	**0.000**	**0.000**	**0.036**
T [s]	**0.000**	**0.000**	0.098
Texture	**0.047**	0.550	**0.002**
P[w] × t [s]	**0.004**	0.421	**0.002**
P[w] × texture	0.119	0.098	0.382
T [s] × texture	0.682	0.414	0.343
P[w] × t [s] × texture	0.150	0.727	0.056
R-sq [%]	*84.78*	*92.64*	*67.62*

3.4. ANOVA analysis

The ANOVA (ANalysis Of VAriance) analysis was applied in order to validate the phenomenologies observed in the previous paragraphs (please refer to Sections 3.1 and 3.2), in terms of effects and joining mechanisms, in order to confirm the significance of the control factors (i.e., laser power, time and texture) for the response variables (i.e., UFS, A and τ), also from a statistical point of view. The results of ANOVA consist of a table containing, for each parameter or parameter combination, the degrees of freedom, the sum of squares, the adjusted sum of squares, the adjusted means squares, and the F value (Fisher-value). The analysis was conducted at a 95 % confidence level (α = 0.05). Thus, a process parameter or a parameter interaction is considered significant when the p-value is less than 0.05. Before the ANOVA analysis, the underlying hypotheses, i.e., the assumptions of normality, independence, additivity, and homogeneous variance, were verified through the graphical analysis of the residuals [50]. Then, the main effect plots were used to assess the relation between the control factors and the joint strength. The interaction plots were additionally examined to highlight the synergic or anti-synergic effect on the response due to the combination of control factors.

Table 7 summarizes the results of the ANOVA analysis on the effect of the factors (i.e., P, t and texture) and their second and third-order interactions on the parameters UFS, A and τ in terms of the p-value. The significant control factors and their interactions are reported in bold (p-value < 0.05). While Figs. 16 to 18 show the main effect and interaction

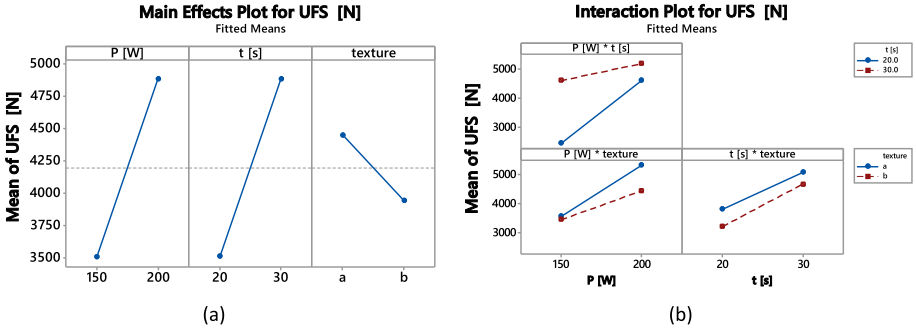

Fig. 16. a) Main effect plot and (b) interaction plot for UFS.

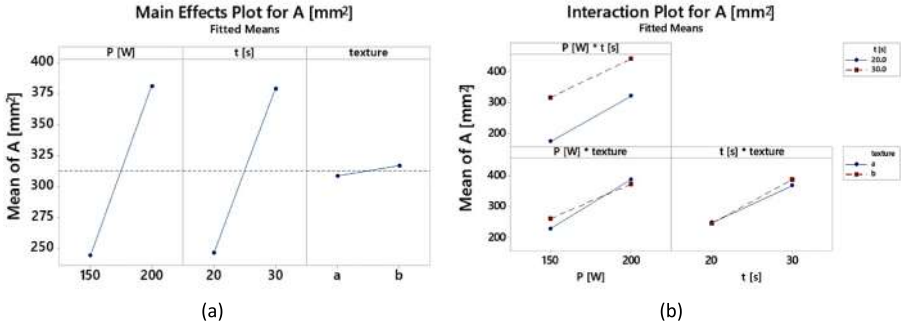

Fig. 17. a) main effect plot and (b) interaction plot for a.

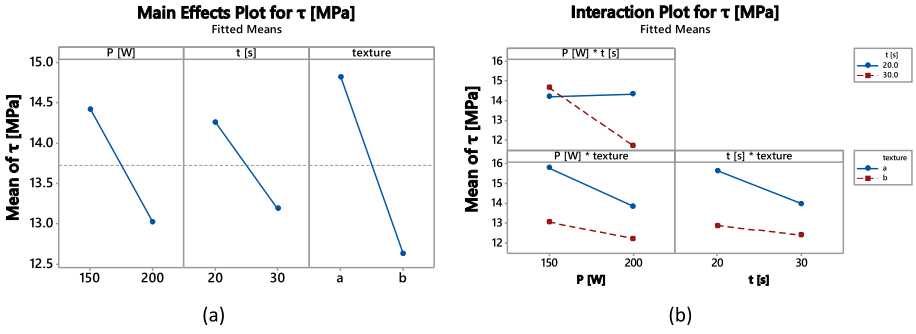

Fig. 18. a) Main effect plot and (b) interaction plot for τ.

plots for all the response variables, in order UFS, A and τ, respectively.

In the studied case, the ANOVA models well fit the experimental data: the R-sq (coefficient of determination) is high in the case of UFS [N] and A [mm^2] (i.e., 84.78 % and 92.64 %, respectively); good in the case of τ (i.e., 67.62 %). It is worth noting that in the latter case, the control factor is a ratio, as defined in eq. (1); consequently, the model considers the error derived by both the dividends.

The ANOVA indicates the statistical significance of all control factors (i.e., P, t and texture) on the UFS response variable; in addition, it asses as significant only the factors' interaction P[w] × t [s], as also visible from the observation of the main effect and interaction plots of Fig. 16. In particular, the increase in the laser power and joining time results in a significant increase in UTS, as stated in Section 3.1, as opposed to the transition from texture A to B. Regarding the A parameter, only the texture among control parameters does not affect the joined area, while the increase in the laser power and joining time results in a significant enlargement of the joining area, confirming the findings in Section 3.1 following visual observation of the joined areas in Fig. 10; in addition, all the factors' interactions are not significant, as also confirmed by the observation in Fig. 17b (the curves are indeed very little incident, almost parallel to each other). Two control factors, i.e., laser power and texture, and the lone interaction P[w] × t [s] affect the apparent shear stress statistically, as can be seen from observing the graphs in Fig. 18. In particular, the increase in the laser power and joining time, as well as the change from texture A to B, determine a significant reduction in τ, with texture having a greater effect than the other two control factors.

4. Conclusions

The study explores the use of laser technology as a sustainable and efficient method for joining titanium and PEEK. The developed setup, i.e., a 200 W diode laser with a beam expander in static conditions, was found to be suitable for the joining process. By varying laser power and time, it is possible to optimize the joint. At high laser energy (i.e., high power and long-time) the degradation of the PEEK can occur at the interface, with bubbles formation, which can limit the strength of the joints.

The optimal conditions were found, resulting in a strong joint with chemical bonding between the materials: the maximum values of UFS of about 6 kN and τ of about 18 MPa were achieved, resulting in joint efficiency of about 30 % (compared to the shear resistance of PEEK). It is worth noting that such value is greater than that achieved with adhesives. From the EDXS analysis, there is evidence of a substantial percentage of Ti and oxygen present on the surface of PEEK, i.e., about 6 and 24 %, respectively, as well as a relevant percentage of oxygen also present on the metal surface, i.e., about 23 %. Highlighting the possible combination of surface oxidation of both titanium and PEEK, with the formation of reactive chemical groups that can chemically bond together.

This new approach offers a promising alternative to traditional adhesive methods, providing a strong, efficient, and more environmentally friendly solution.

CRediT authorship contribution statement

Silvio Genna: Writing – review & editing, Resources, Project administration, Methodology, Investigation, Data curation, Conceptualization. **Patrizia Moretti:** Writing – original draft, Investigation, Formal analysis, Data curation. **Gennaro Salvatore Ponticelli:** Writing – review & editing, Investigation, Formal analysis, Data curation. **Simone Venettacci:** Writing – review & editing, Validation, Investigation, Formal analysis, Data curation.

Funding

This study has been funded through the Programma Operativo Regionale – POR FESR Lazio 2014–2020, Call "Gruppi di Ricerca 2020″, Project A0375 – 2020—36716 "Laser joIning fOr New hybrid Structures – LIONS" – CUP: E85F21000820005.

Declaration of competing interest

The authors declare that they have no known competing financial interests or personal relationships that could have appeared to influence the work reported in this paper.

Data availability

Data will be made available on request.

References

[1] C. Lamberti, T. Solchenbach, P. Plapper, W. Possart, Laser assisted joining of hybrid polyamide-aluminum structures, Phys. Procedia 56 (2014) 845–853, https://doi.org/10.1016/J.PHPRO.2014.08.103.
[2] Y. Huang, X. Gao, Y. Zhang, B. Ma, Laser joining technology of polymer-metal hybrid structures - a review, J. Manuf. Process. 79 (2022) 934–961, https://doi.org/10.1016/j.jmapro.2022.05.026.
[3] F. Lambiase, S. Genna, Laser-assisted direct joining of AISI304 stainless steel with polycarbonate sheets: thermal analysis, mechanical characterization, and bonds morphology, Opt. Laser Technol. 88 (2017) 205–214, https://doi.org/10.1016/J.OPTLASTEC.2016.09.028.
[4] M.K. Raymond, Adhesives get in the groove, Mach. Des. (1998).
[5] Y. Liu, X. Wang, L. Zhou, H. Zhao, X. Han, C. Tan, X. Song, Achievement of high-strength Al/CFRP hybrid joint via high-speed friction stir lap joining and laser texturing pretreatment parameters variation, Thin-Walled Struct. 199 (2024) 111762, https://doi.org/10.1016/J.TWS.2024.111762.
[6] M.J. Troughton, ed., Mechanical Fastening, in: Handbook of Plastics Joining, Second Edi, Elsevier, 2009: pp. 175–201. doi: 10.1016/B978-0-8155-1581-4.50020-2.
[7] D.W. Oplinger, Mechanical Fastening and Adhesive Bonding, in: Handbook of Composites, Springer US, Boston, MA, 1998: pp. 610–666. doi: 10.1007/978-1-4615-6389-1_29.
[8] J.-H. Kweon, J.-W. Jung, T.-H. Kim, J.-H. Choi, D.-H. Kim, Failure of carbon composite-to-aluminum joints with combined mechanical fastening and adhesive bonding, Compos. Struct. 75 (2006) 192–198, https://doi.org/10.1016/j.compstruct.2006.04.013.
[9] F. Yusof, F. Jamaludin, M. Abd Shukor, A brief review: laser joining of polymer-metal structures, ASEAN Eng. J. Part A 2 (2012) 5–12, https://doi.org/10.11113/AEJ.V2.15345.
[10] Y. Huang, X. Meng, Y. Xie, L. Wan, Z. Lv, J. Cao, J. Feng, Friction stir welding/processing of polymers and polymer matrix composites, Compos. A Appl. Sci. Manuf. 105 (2018) 235–257, https://doi.org/10.1016/J.COMPOSITESA.2017.12.005.
[11] F. Lambiase, A. Paoletti, V. Grossi, A. Di Ilio, Friction assisted joining of aluminum and PVC sheets, J. Manuf. Process. 29 (2017) 221–231, https://doi.org/10.1016/J.JMAPRO.2017.07.026.
[12] F. Lambiase, S. Genna, Moisture-induced defects produced by direct laser joining of AA7075 aluminum and PEEK, Opt. Laser Technol. 165 (2023) 109553, https://doi.org/10.1016/J.OPTLASTEC.2023.109553.
[13] A. Ozlati, M. Movahedi, M. Tamizi, Z. Tartifzadeh, S. Alipour, An alternative additive manufacturing-based joining method to make metal/polymer hybrid structures, J. Manuf. Process. 45 (2019) 217–226, https://doi.org/10.1016/J.JMAPRO.2019.07.002.
[14] Y.H. Chueh, C. Wei, X. Zhang, L. Li, Integrated laser-based powder bed fusion and fused filament fabrication for three-dimensional printing of hybrid metal/polymer objects, Addit. Manuf. 31 (2020) 100928, https://doi.org/10.1016/J.ADDMA.2019.100928.
[15] S. Genna, P. Moretti, G.S. Ponticelli, S. Venettacci, Laser-based thermomechanical joining of semi-transparent thermoplastics with technical steel, Int. J. Adv. Manuf. Technol. 132 (2024) 3735–3755, https://doi.org/10.1007/s00170-024-13624-6.
[16] S. Katayama, Laser Welding, Joining, or Brazing of Dissimilar Materials, in: Fundamentals and Details of Laser Welding, Springer Singapore, Singapore, 2020, pp. 167–184, https://doi.org/10.1007/978-981-15-7933-2_9.
[17] K. Schricker, L. Samfaß, M. Grätzel, G. Ecke, J.P. Bergmann, Bonding mechanisms in laser-assisted joining of metal-polymer composites, J. Adv. Join. Process. 1 (2020) 100008, https://doi.org/10.1016/J.JAJP.2020.100008.
[18] V. Wippo, P. Jaeschke, M. Brueggmann, O. Suttmann, L. Overmeyer, Advanced laser transmission welding strategies for fibre reinforced thermoplastics, in: Phys Procedia, Elsevier, 2014, pp. 1191–1197, https://doi.org/10.1016/j.phpro.2014.08.034.
[19] S. Katayama, Y. Kawahito, Laser direct joining of metal and plastic, Scr. Mater. 59 (2008) 1247–1250, https://doi.org/10.1016/j.scriptamat.2008.08.026.
[20] S.J. Adarsh, A. Natarajan, Studies on process parameter optimization and surface modification for joint strength enhancement of laser welded Aluminium 5754-Polyamide hybrid joints, Mater. Today Commun. 37 (2023) 107198, https://doi.org/10.1016/J.MTCOMM.2023.107198.

[21] C.W. Chan, G.C. Smith, Fibre laser joining of highly dissimilar materials: commercially pure Ti and PET hybrid joint for medical device applications, Mater. Des. 103 (2016) 278–292, https://doi.org/10.1016/j.matdes.2016.04.086.
[22] F.I. Hussein, E. Akman, B. Genc Oztoprak, M. Gunes, O. Gundogdu, E. Kacar, K. I. Hajim, A. Demir, Evaluation of PMMA joining to stainless steel 304 using pulsed Nd:YAG laser, Opt. Laser Technol. 49 (2013) 143–152, https://doi.org/10.1016/j.optlastec.2012.12.028.
[23] G.L. Georgiev, R.J. Baird, E.F. McCullen, G. Newaz, G. Auner, R. Patwa, H. Herfurth, Chemical bond formation during laser bonding of Teflon ® FEP and titanium, Appl. Surf. Sci. 255 (2009) 7078–7083, https://doi.org/10.1016/j.apsusc.2009.03.046.
[24] F. Yusof, M. Yukio, M. Yoshiharu, M.H. Abdul Shukor, Effect of anodizing on pulsed Nd:YAG laser joining of polyethylene terephthalate (PET) and aluminium alloy (A5052), Mater. Des. 37 (2012) 410–415, https://doi.org/10.1016/j.matdes.2012.01.006.
[25] P. Amend, S. Pfindel, M. Schmidt, Thermal joining of thermoplastic metal hybrids by means of mono- and polychromatic radiation, Phys. Procedia 41 (2013) 98–105, https://doi.org/10.1016/J.PHPRO.2013.03.056.
[26] K. Schricker, M. Stambke, J.P. Bergmann, K. Bräutigam, Laser-based joining of thermoplastics to metals: influence of varied ambient conditions on joint performance and microstructure, Int J Polym Sci 2016 (2016), https://doi.org/10.1155/2016/5301081.
[27] T. Sinmazçelik, E. Avcu, M.Ö. Bora, O. Çoban, A review: fibre metal laminates, background, bonding types and applied test methods, Mater. Des. 32 (2011) 3671–3685, https://doi.org/10.1016/J.MATDES.2011.03.011.
[28] W.-H. Tsai, Y.-C. Chang, S.-J. Lin, H.-C. Chen, P.-Y. Chu, A green approach to the weight reduction of aircraft cabins, J. Air Transp. Manag. 40 (2014) 65–77, https://doi.org/10.1016/j.jairtraman.2014.06.004.
[29] M. Kalanchiam, M. Chinnasamy, Advantages of composite materials in aircraft structures, international journal of mechanical, aerospace, industrial, mechatronic and manufacturing, Engineering 6 (2012) 2428–2432.
[30] G.S. Ponticelli, S. Venettacci, F. Tagliaferri, S. Guarino, Fused deposition modelling for aeronautics: techno-economic and environmental assessment for overhead locker supports replacement, Int. J. Adv. Manuf. Technol. 128 (2023) 3817–3840, https://doi.org/10.1007/s00170-023-12135-0.
[31] F. Tanasa, M. Zanoaga, Fiber-reinforced polymer composites as structural materials for aeronautics, Int. Conf. Scientific Paper AFASES (2013) 1–10. http://www.newairplane.com/787.
[32] R. Alderliesten, On the development of hybrid material concepts for aircraft structures, Recent Pat. Eng. 3 (2009) 25–38, https://doi.org/10.2174/187221209787259893.
[33] E. Grossman, I. Gouzman, Space environment effects on polymers in low earth orbit, In: Nucl Instrum Methods Phys Res B, North-Holland, 2003: pp. 48–57. doi: 10.1016/S0168-583X(03)00640-2.
[34] E.M. Silverman, Space environmental effects on spacecraft: LEO materials selection guide (Part 2), NASA Tech. Memo. (1995).
[35] J. Shi, G. Ma, C. Han, G. Li, Y. Liu, Q. Liu, Tribological properties and bearing application of Mo-based films in space environment, Vacuum 188 (2021) 110217, https://doi.org/10.1016/J.VACUUM.2021.110217.
[36] A. Gisario, M. Mehrpouya, S. Venettacci, M. Barletta, Laser-assisted bending of Titanium Grade-2 sheets: experimental analysis and numerical simulation, Opt. Lasers Eng. 92 (2017), https://doi.org/10.1016/j.optlaseng.2016.09.004.
[37] J. Kleiman, Protection of materials and structures from space environment – ICPMSE proceedings series: How did it all start?, in: Astrophysics and Space Science Proceedings Springer, Netherlands, 2013, pp. 1–12, https://doi.org/10.1007/978-3-642-30229-9_1.
[38] G. Reyes, H. Kang, Mechanical behavior of lightweight thermoplastic fiber-metal laminates, J. Mater. Process. Technol. 186 (2007) 284–290, https://doi.org/10.1016/j.jmatprotec.2006.12.050.
[39] H. Wang, Z. Ren, Y. Guan, Laser joining of continuous carbon fiber-reinforced PEEK and titanium alloy with high strength, Polymers (Basel) 14 (2022), https://doi.org/10.3390/polym14214676.
[40] C. Tan, J. Su, B. Zhu, X. Li, L. Wu, B. Chen, X. Song, J. Feng, Effect of scanning speed on laser joining of carbon fiber reinforced PEEK to titanium alloy, Opt. Laser Technol. 129 (2020) 106273, https://doi.org/10.1016/J.OPTLASTEC.2020.106273.
[41] H. Wang, P. Yan, X. Ding, Y. Guan, Enhanced laser direct joining of continuous carbon fiber reinforced polyetheretherketone and titanium alloy with controllable mechanical interlocks, J. Manuf. Process. 86 (2023) 56–65, https://doi.org/10.1016/J.JMAPRO.2022.12.051.
[42] P. Zou, H. Zhang, M. Lei, D. Cheng, Formation mechanism of direct laser welding joint between CFRTP and Ti-6Al-4V, Mater. Lett. 325 (2022) 132707, https://doi.org/10.1016/J.MATLET.2022.132707.
[43] P. Zou, H. Zhang, M. Lei, D. Cheng, S. Huang, F. Yang, Interfacial microstructure and formation of direct laser welded CFRP/Ti-6Al-4V joint, Metals (Basel) 11 (2021), https://doi.org/10.3390/met11091398.
[44] M. Di Siena, S. Genna, P. Moretti, G.S. Ponticelli, S. Venettacci, P. Russo, Study of the laser-material interaction for innovative hybrid structures: thermo-mechanical characterization of polyethylene-based polymers, Polym. Test. 120 (2023), https://doi.org/10.1016/j.polymertesting.2023.107947.
[45] F. Lambiase, A. Paoletti, Mechanical behavior of AA5053/polyetheretherketone (PEEK) made by friction assisted joining, Compos. Struct. 189 (2018) 70–78, https://doi.org/10.1016/j.compstruct.2018.01.045.
[46] S. Genna, E. Menna, G. Rubino, F. Trovalusci, Laser machining of silicon carbide: experimental analysis and multiobjective optimization, Ceram. Int. 49 (2023) 10682–10691, https://doi.org/10.1016/J.CERAMINT.2022.11.258.
[47] F. Lambiase, S. Genna, R. Kant, A procedure for calibration and validation of FE modelling of laser-assisted metal to polymer direct joining, Opt. Laser Technol. 98 (2018) 363–372, https://doi.org/10.1016/j.optlastec.2017.08.016.
[48] F. Lambiase, S. Genna, C. Leone, A. Paoletti, Laser-assisted direct-joining of carbon fibre reinforced plastic with thermosetting matrix to polycarbonate sheets, Opt. Laser Technol. 94 (2017) 45–58, https://doi.org/10.1016/j.optlastec.2017.03.006.
[49] J.A.M. Ferreira, R.D.S.G. Campilho, M.G. Cardoso, F.J.G. Silva, Numerical simulation of adhesively-bonded T-stiffeners by cohesive zone models, in, Procedia Manuf, Elsevier BV (2020) 870–877, https://doi.org/10.1016/j.promfg.2020.10.122.
[50] D.C. Montgomery, Design and analysis of experiments, n.d.